Molecular Cell
Article

A Mammalian Pre-mRNA 5′ End Capping Quality Control Mechanism and an Unexpected Link of Capping to Pre-mRNA Processing

Xinfu Jiao,[1,5] Jeong Ho Chang,[2,3,5] Turgay Kilic,[2,4] Liang Tong,[2,*] and Megerditch Kiledjian[1,*]
[1]Department Cell Biology and Neuroscience, Rutgers University, Piscataway, NJ 08854, USA
[2]Department Biological Sciences, Columbia University, New York, NY 10027, USA
[3]Present Address: Department of Biomedical Science, Daegu University, Gyeongsan 712-714, South Korea
[4]Present Address: Department of Biochemistry, University of Texas Health Science Center, San Antonio, TX 78229, USA
[5]These authors contributed equally to this work
*Correspondence: ltong@columbia.edu (L.T.), kiledjian@biology.rutgers.edu (M.K.)
http://dx.doi.org/10.1016/j.molcel.2013.02.017

SUMMARY

Recently, we reported that two homologous yeast proteins, Rai1 and Dxo1, function in a quality control mechanism to clear cells of incompletely 5′ end-capped messenger RNAs (mRNAs). Here, we report that their mammalian homolog, Dom3Z (referred to as DXO), possesses pyrophosphohydrolase, decapping, and 5′-to-3′ exoribonuclease activities. Surprisingly, we found that DXO preferentially degrades defectively capped pre-mRNAs in cells. Additional studies show that incompletely capped pre-mRNAs are inefficiently spliced at all introns, a fact that contrasts with current understanding, and are also poorly cleaved for polyadenylation. Crystal structures of DXO in complex with substrate mimic and products at a resolution of up to 1.5Å provide elegant insights into the catalytic mechanism and molecular basis for their three apparently distinct activities. Our data reveal a pre-mRNA 5′ end capping quality control mechanism in mammalian cells, indicating DXO as the central player for this mechanism, and demonstrate an unexpected intimate link between proper 5′ end capping and subsequent pre-mRNA processing.

INTRODUCTION

The 5′ end 7-methylguanosine (m^7G) cap of eukaryotic messenger RNAs (mRNAs) is the first modification of nascent transcripts (pre-mRNAs) shortly after the initiation of transcription, and it plays critical roles in mRNA biogenesis and stability (Furuichi and Shatkin, 2000; Ghosh and Lima, 2010; Liu and Kiledjian, 2006; Merrick, 2004; Meyer et al., 2004; Shatkin, 1976). The N^7 methyl group on the cap is essential for recognition by the cap-binding proteins CBP20 and eIF4E (Fischer, 2009; Gingras et al., 1999; Goodfellow and Roberts, 2008) and for efficient splicing, polyadenylation, mRNA export, and translation. Removal of the 5′ end cap is catalyzed by the Dcp2 (Dunckley and Parker, 1999; Lykke-Andersen, 2002; Wang et al., 2002) and Nudt16 (Li et al., 2011; Song et al., 2010) decapping enzymes, releasing m^7 guanosine diphosphate (GDP) and 5′ monophosphate RNA. Decapping is associated with mRNA decay, turnover, and quality control because the 5′ monophosphorylated RNA is rapidly degraded by the cytoplasmic, processive 5′-to-3′ exoribonuclease Xrn1 (Decker and Parker, 1993; Hsu and Stevens, 1993). In contrast, the primary transcripts, including the 5′ end triphosphate group, and other capping intermediates cannot serve as substrates for the classical decapping enzymes and would be protected from degradation by the 5′-to-3′ exoribonucleases. Therefore, it was generally believed that the capping process always proceeded to completion.

Our recent studies on the yeast protein Rai1 and its homolog Dxo1 (Ydr370C) have demonstrated new catalytic activities that can remove incomplete caps from mRNAs, indicating that capping may be less efficient than initially thought. Specifically, Rai1 possesses RNA 5′ pyrophosphohydrolase (PPH) activity, hydrolyzing the 5′ end triphosphate to release pyrophosphates (Xiang et al., 2009). Rai1 also has a distinct "decapping" activity, hydrolyzing the entire cap structure from an unmethylated 5′ end-capped RNA to release GpppN (Jiao et al., 2010). In comparison, Dxo1 lacks PPH activity, but it does possess decapping activity on both methylated and unmethyl-capped RNAs (Chang et al., 2012).

The identification of such catalytic activities suggests the hypothesis that mRNAs with incomplete 5′ end caps are produced in yeast and that Rai1 and Dxo1 function as quality control mechanisms to mediate the clearance of such defective mRNAs. In fact, the catalytic activities of Rai1 and Dxo1 ultimately generate RNAs with 5′ end monophosphate, which can be readily degraded by 5′-to-3′ exoribonucleases. Dxo1 also possesses a distributive 5′-to-3′ exoribonuclease activity, enabling this enzyme to single-handedly decap and degrade incompletely capped mRNAs (Chang et al., 2012).

Studies in yeast cells have confirmed the existence of this mRNA 5′ end capping quality control. Unmethylated 5′ end-capped mRNAs were more stable in cells with a deleted *Rai1* gene, and the exposure of these cells to nutrient stress

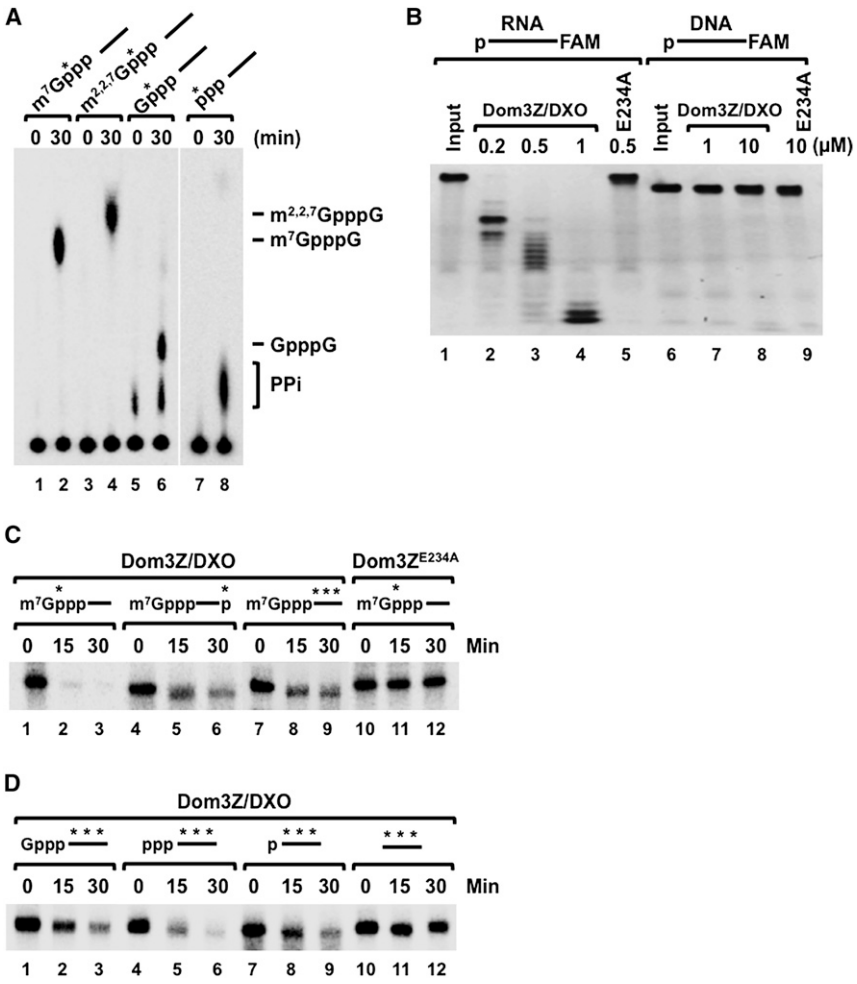

Figure 1. Dom3Z/DXO Possesses Pyrophosphohydrolase, Decapping, and 5′-to-3′ Exoribonuclease Activities

(A) The decapping activity of Dom3Z/DXO toward RNAs with various 5′ ends is depicted schematically at the top and shown where the RNA is represented by a line. The asterisk denotes the ^{32}P position. Reactions were carried out with 25 nM pcP RNA and 25 nM recombinant His-tagged Dom3Z protein at 37°C for the indicated times. Decapping products were resolved on PEI-TLC developed in 0.45 M $(NH_4)_2SO_4$ (lanes 1–6) or 0.75 M KH_2PO_4 ([pH 3.4]; lanes 7 and 8). The migrations of cap analog markers are indicated.

(B) Wild-type (WT) and mutant Dom3Z/DXO proteins were incubated with 5′ end monophosphate 30 nt RNA or DNA substrates labeled at the 3′ end with the FAM (6-carboxyfluorescein) fluorophore. The remaining RNA or DNA fragments were resolved by 5% denaturing PAGE and visualized under UV light, confirming the distributive, 5′-to-3′ exoribonuclease activity. The RNA or DNA is denoted by a line, and the 5′ monophosphate is represented by the p at the beginning of the line. The catalytically inactive E234A mutant is shown.

(C) In vitro decay reactions were carried out with 100 nM recombinant His-tagged Dom3Z/DXO for the indicated times with methyl-capped RNAs (25 nM) represented schematically with the ^{32}P labeling indicated by the asterisk. The remaining RNAs were resolved by 5% denaturing PAGE. Catalytically inactive Dom3Z/DXO mutant (Dom3Z^{E234A}) was used as a negative control.

(D) The 5′ end substrate specificity of Dom3Z/DXO was tested as in (A) with RNAs containing distinct 5′ ends denoted schematically. RNAs with a 5′ hydroxyl were not degraded by Dom3Z/DXO.

generated mRNAs with incompletely capped 5′ ends (Jiao et al., 2010). More importantly, yeast cells in which both *Rai1* and *Dxo1* were disrupted produced mRNAs with incomplete caps, even under normal growth conditions (Chang et al., 2012). It appears that fungi possess two partially redundant proteins that can detect and degrade incompletely capped mRNAs, which are generated under both stress and nonstress conditions.

Rai1 and Dxo1 have a weak sequence homolog known as Dom3Z in mammals (Xue et al., 2000). Dom3Z has a similar three-dimensional structure (Xiang et al., 2009), but its biochemical activities and biological functions have not been characterized. Here, we report that Dom3Z possesses PPH, decapping, and exoribonuclease activities. Crystal structures of Dom3Z in complex with substrate mimic and products at a resolution of up to 1.5Å provide elegant insights into the catalytic mechanism and the molecular basis for the three apparently distinct activities of these enzymes. Importantly, Dom3Z preferentially functions on incompletely capped pre-mRNAs. Our studies also reveal unexpected insights into the connection between 5′ end capping and splicing, showing that defective capping inhibits splicing at internal introns, whereas current data suggest that the cap affects the splicing of only the first intron.

RESULTS

Dom3Z/DXO Has Decapping, PPH, and Exonuclease Activities

Mammalian Dom3Z is a weak sequence homolog of yeast Rai1 and Dxo1 but has a strong structural similarity to both (Chang et al., 2012; Xiang et al., 2009). Therefore, we tested which biochemical activities Dom3Z shares with Rai1 and Dxo1. Mouse Dom3Z (Figure S1 available online) readily decapped unmethylcapped RNA (GpppG-RNA) to release the GpppG cap structure (Figure 1A; lanes 5 and 6), and it possessed PPH activity as well, releasing PP_i from triphosphate RNA (pppRNA) (lanes 7 and 8). Interestingly, Dom3Z also showed strong decapping activity toward both monomethylated (lanes 1 and 2) and trimethylated (lanes 3 and 4) capped RNAs. The observed activities are a function of Dom3Z, given that two different mutations within the putative active site (E234A and D236A) abrogated the decapping activity (Figure S2). These data demonstrate that Dom3Z possesses decapping and PPH activities on incompletely capped mRNAs and also functions on m^7G- and $m^{2,2,7}G$-capped mRNAs.

Next, we tested whether Dom3Z also possesses 5′-to-3′ exoribonuclease activity, on the basis of our observations with Dxo1 (Chang et al., 2012). A 30 nt RNA substrate with a 5′ end

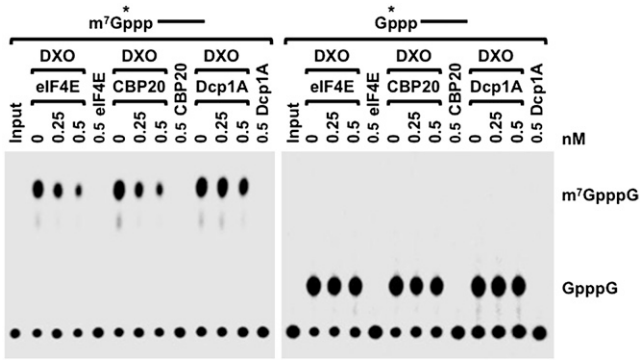

Figure 2. Cap-Binding Proteins Compete for DXO Decapping on Methyl-Capped RNA In Vitro

Decapping activity of 20 nM DXO on ^{32}P 5′ end-labeled, methyl-capped, or unmethyl-capped RNA in the presence of the indicated eIF4E, CBP20, or Dcp1A proteins are shown. Decapping assay was carried out as described in Figure 1. Both eIF4E and CBP20 can inhibit DXO decapping on methyl-capped, but not unmethyl-capped, RNA.

monophosphate and a 3′ end FAM (6-carboxyfluorescein) fluorophore (Sinturel et al., 2009) was degraded by wild-type (WT) Dom3Z from the 5′ end, with clear intermediates being detected (Figure 1B; lanes 2–4), but not by a catalytically inactive Dom3Z (lane 5), suggesting that Dom3Z has distributive 5′-to-3′ exoribonuclease activity. The lack of detectable activity on a single-stranded DNA (ssDNA) substrate (lanes 6–9) demonstrated that Dom3Z exonuclease activity is RNA-specific.

To determine whether capped RNAs can be degraded by Dom3Z, we incubated 5′ end-labeled, 3′ end-labeled, or uniformly labeled methyl-capped RNAs with Dom3Z and measured their decay over time in vitro. All the RNAs were efficiently degraded by Dom3Z (Figure 1C). Dom3Z activity was also tested on RNAs with different 5′ end modifications, which included an unmethylated cap, a triphosphate group, a monophosphate group, and a hydroxyl group. All the substrates except one with a 5′ end hydroxyl were degraded (Figure 1D), demonstrating that the Dom3Z 5′-to-3′ exonuclease activity requires a 5′ end monophosphate on the RNA substrate, which is analogous to the exonuclease activities of Xrn1 and Xrn2.

Overall, our data demonstrate that Dom3Z has three catalytic activities: decapping activity that removes the entire methylated or unmethylated cap structure, PPH activity, and distributive 5′-to-3′ exonuclease activity. Henceforth, we will refer to Dom3Z as decapping exoribonuclease (DXO).

Although DXO showed decapping activity toward methyl-capped RNAs in vitro, we suspected that such an activity would be thwarted in cells by cap-binding proteins, which preferentially bind the methylated cap (Calero et al., 2002; Marcotrigiano et al., 1997; Matsuo et al., 1997; Mazza et al., 2002) and thereby can protect the RNA against decapping by DXO. Consistent with this hypothesis, both the nuclear and the cytoplasmic cap-binding proteins, CBP20 and eIF4E (Figure S1), efficiently inhibited DXO decapping of methyl-capped RNA in vitro but had no protective effect on unmethyl-capped RNA (Figure 2). These data indicate that DXO should preferentially target defectively capped RNAs in cells.

Crystal Structure of DXO in Complex with an RNA Oligonucleotide Product

DXO, Rai1, and Dxo1 have three apparently distinct catalytic activities—RNA 5′ end PPH, decapping, and 5′-to-3′ exoribonuclease—though a common product, the RNA body with a 5′ end monophosphate, is generated by these activities. Although our biochemical data suggest that these activities are mediated by a common active site, the molecular mechanism for them is not clear. These proteins share four conserved sequence motifs in the putative active site region (Chang et al., 2012), corresponding to residues Arg132 (motif I), Glu192 (motif II, GΦxΦE, where Φ is an aromatic or hydrophobic residue and x is any residue), Glu234 and Asp236 (motif III, EhD, where h is a hydrophobic residue), and Glu253 and Lys255 (motif IV, EhK) in mouse DXO (Figure S3). Residues Glu192, Asp236, and Glu253 are known to coordinate an Mg^{2+} ion in the active site (through a water molecule for Glu192) (Xiang et al., 2009). The functional roles of the other conserved residues in substrate binding and/or catalysis are not known.

To understand the catalytic mechanism(s) of these enzymes, we determined the crystal structure of WT mouse DXO in complex with magnesium ions and an RNA penta-nucleotide with a 5′ end phosphate, pU5, at a resolution of 1.8 Å (Figure 3A). We prepared the complex by soaking crystals of DXO free-enzyme with a solution containing 10 mM pU5 and 10 mM $MgCl_2$ for 90 min. The structure had an excellent agreement with the X-ray diffraction data and the expected bond lengths, bond angles, and other geometric parameters (Table 1).

Clear electron density was observed for the first three nucleotides of pU5 (Figure 3B). The remaining two nucleotides had weaker electron density, and there was a break in the electron density between the third and fourth nucleotide. The structural analysis suggests that the pU5 RNA is bound in the active site of DXO as a product of this enzyme; the 5′ end phosphate being the scissile phosphate of the substrate (see below). Hence, the nucleotides are numbered from two to six (Figure 3C), with the expectation that nucleotide 1 would be the leaving group in the substrate. Although pU5 can serve as a substrate for the 5′-to-3′ exonuclease activity of DXO, its binding mode in the current crystal is consistent with that of a product of this activity.

The first nucleotide of the oligo, U_2, has extensive interactions with DXO, especially the 5′ end phosphate group (see below). The rest of the oligo runs along strand β12, and there are two hydrogen bonds between the main chain amides of this β strand (residues 256 and 258) and the backbone phosphate groups of the oligo (U_3 and U_4) (Figure 3C). In addition, three positively charged side chains, Lys258, Lys273, and Arg294, interact with the phosphate groups of the RNA, Lys273 and Arg294 being conserved among the DXO, Rai1, and Dxo1 homologs (Figure S3). On the other hand, the bases of the nucleotides are not recognized specifically by DXO, and they have weaker electron density as well (Figure 3B), consistent with our biochemical data showing that DXO does not have sequence specificity. The active site pocket is only large enough to accommodate a single-stranded substrate (Figure 3D), and we observed earlier that Dxo1 stalls at double-stranded portions of the substrate (Chang et al., 2012).

Unexpectedly, the structure reveals that a second metal ion is bound in the active site in the presence of the pU5 oligo (Figure 3E). Both metal ions are located in an octahedral coordination sphere. The first metal ion (Mg1) is in the same position that was observed earlier in the free enzyme (Xiang et al., 2009), whereas binding of the second metal ion (Mg2) is possible only in the presence of the RNA, given that one of the terminal oxygen atoms on the 5′ end phosphate of the RNA is a bridging ligand to both metal ions. The side chain of Asp236 (motif III) makes a bidentate coordination of both metal ions, and the side chain of Glu192 (motif II) makes a hydrogen bond to one water ligand on each of the metal ions. Mg1 is also coordinated by the side chain of Glu253 (motif IV), the main-chain carbonyl of residue 254, as well as another terminal oxygen atom of the 5′ end phosphate group of the RNA. Therefore, this phosphate group replaces two of the water ligands of Mg1 in the free enzyme (Xiang et al., 2009). For Mg2, the side chain of Glu234 (the second acidic residue of motif III) and two additional water molecules complete the octahedral coordination.

The ribose of U_2 is packed against the side chain of Tyr189 (motif II) (Figures 3C and S4). This residue is most often a phenthalanine or tyrosine (Tyr) among these enzymes. In addition, the 2′ hydroxyl group of the ribose is hydrogen-bonded to the main-chain carbonyl of residue 185 (Figure S4). This residue is in the middle of helix αD, but a small kink in the helix in this region makes the carbonyl oxygen available for hydrogen bonding to the ribose.

Crystal Structure of DXO in Complex with an RNA Oligonucleotide Substrate Mimic

To observe the binding mode of the 5′ end nucleotide of a substrate RNA in the DXO active site, we used a hexanucleotide with a 5′ end monophosphate and with the phosphodiester group between nucleotides 1and 2 and 2 and 3 replaced with a phosphorothioate group to inhibit the hydrolysis of this RNA. Therefore, this pU(S)6 oligonucleotide had the sequence pU_1-$^{S}U_2$-$^{S}U_3$-U_4-U_5-U_6. In addition, we replaced the Mg^{2+} ion with a Ca^{2+} ion during crystallization to further block hydrolysis of the RNA. Our enzymatic assays showed that DXO is essentially inactive, Ca^{2+} being the divalent metal ion (data not shown).

We have determined the crystal structure of mouse DXO in complex with Ca^{2+} and the pU(S)6 oligonucleotide at a resolution of 1.7 Å (Table 1 and Figure S5). Clear electron density was observed for the first four nucleotides of the RNA (Figure 3F). Very weak electron density was observed for the bases of the last two nucleotides, and they were not included in the atomic model.

The RNA is bound in the active site with the phosphorothioate group between nucleotides 1 and 2 located next to the catalytic site (Figure 3G). The 5′ end phosphate group of the oligo interacts with the side chain of Arg132 (motif I), and it is also close to the side chain of Gln280 (Figure 3G). The base of the first nucleotide maintains π-stacking with that of the second nucleotide. The binding modes of nucleotides 2–4 are highly similar to those of their equivalents in the pU5 complex (Figure S5).

Only one Ca^{2+} ion was observed in the complex, at the same position as Mg1 in the pU5 complex (Figure 3G). The terminal oxygen atom of the phosphorothioate linkage between nucleotides 1 and 2 is a ligand to the metal ion. The conformation of this phosphorothioate group is different from that of the 5′ end phosphate group of the pU5 complex (Figure 3H), equivalent to a ~60° rotation around the O_5-P bond. The sulfur atom in pU(S)6 cannot have a strong interaction with the metal ion and may have (at least partly) driven this conformational change. In fact, this sulfur atom is positioned farthest away from the metal ion (Figure 3G). Besides the phosphorothioate group, a conformational change in the Tyr189 side chain is also observed in the pUS(6) complex, resulting from the presence of the U_1 base (Figure 3H). In addition, the side chain of Glu234 assumes a different conformation, resulting from the absence of the second metal ion.

Although the first nucleotide of the pU(S)6 RNA may mimic the 5′ end of the RNA substrate in terms of exonuclease activity, the phosphorothioate group between nucleotides 1 and 2 is not in the correct conformation for catalysis. The water molecule (or hydroxide ion) that would need to attack the phosphorus atom would not be in the correct position to be activated by any functional group in the active site (Figure 3G). Therefore, conformational changes are expected in this phosphate group, and possibly those atoms that are covalently attached to it, to make this a true substrate. The conformation of the 5′ end phosphate in the pU5 oligo might be a better mimic for the scissile phosphate group.

Crystal Structure of DXO in Complex with the m^7GpppG Cap

To understand how the RNA cap is recognized by DXO, we determined the structure of the WT murine DXO in complex with m^7GpppG at a resolution of 1.5 Å (Table 1 and Figure 4A). There are only a few conformational differences in the active site region between this structure and the one in complex with pU5, the most important of which is the side chain of Glu234. This side chain is somewhat disordered in the cap complex as well as in the free enzyme, and it becomes well-ordered as a ligand to Mg2 in the pU5 complex.

The m^7Gpp group of the cap has good electron density (Figure 4B) and is bound in the active site region at a position similar to that of GDP observed earlier (Xiang et al., 2009) (Figure 4C). The 7-methyl group of guanine is not recognized specifically by the enzyme, which is consistent with our biochemical data showing that DXO is nonselective with regard to the methylation status of the cap (Figure 1A). In fact, residues that contact this guanine base are not well conserved among the enzymes (Figure S3). The ribose is packed against the side chain of Trp131, the residue just preceding motif I, which is conserved as an aromatic residue in most DXO and Rai1 homologs (Figure S3). One of the terminal oxygen atoms on the α-phosphate has ionic interactions with the side chain of Arg132 (motif I) and is hydrogen-bonded to the main-chain amide of Glu234, whereas the other terminal oxygen atom is hydrogen-bonded to the main chain amide of Arg132 at the N-terminal end of helix αB. Therefore, the α-phosphate also has favorable interactions with the dipole of this helix. The β-phosphate is located near the side chains of Arg132 and Gln280, and, in fact, this β-phosphate overlaps with the 5′ end phosphate of the pU(S)6 nucleotide (Figure 3H).

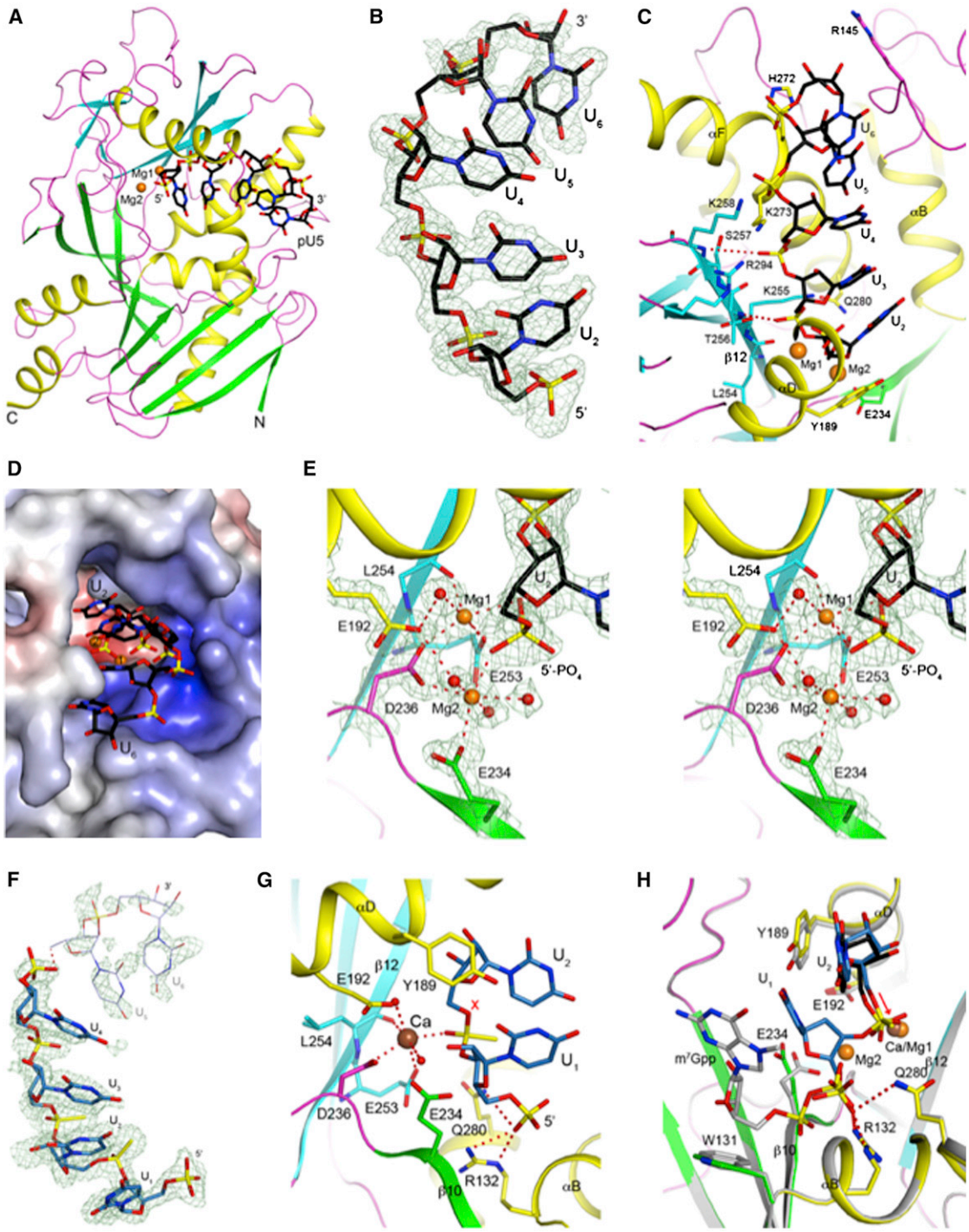

Figure 3. Crystal Structure of Wild-Type Murine DXO in Complex with pU5 and Two Mg^{2+} Ions

(A) A schematic drawing of the structure of DXO (in green for the large β sheet, cyan for the small β sheet, yellow for the helices, and magenta for the loops) in complex with a pU5 RNA oligonucleotide (in black for carbon atoms) and Mg^{2+} ions (orange).

(B) Simulated annealing omit F_o–F_c electron density at a resolution of 1.8 Å for pU5 contoured at 2.5σ.

(C) Interactions between the pU5 RNA with the DXO active site.

(D) The molecular surface of the active site region of DXO. The pU5 RNA is shown as sticks.

(E) The coordination spheres of the two Mg^{2+} ions and the detailed interactions between the 5′ end phosphate group of pU5 and the two Mg^{2+} ions.

(F) Simulated annealing omit F_o–F_c electron density at a resolution of 1.7 Å for pU(S)6 contoured at 2.2σ. Very weak electron density is observed for the last two nucleotides, and they are not included in the atomic model.

(legend continued on next page)

Table 1. Summary of Crystallographic Information

Structure	pU5-Mg^{2+} complex	pU(S)6-Ca^{2+} complex	m^7GpppG complex
Resolution range (Å)[a]	30–1.8 (1.86–1.8)	30–1.7 (1.76–1.7)	40–1.5 (1.55–1.5)
Number of observations	123,120	156,109	274,259
Redundancy	3.2 (2.7)	3.4 (2.9)	4.1 (3.6)
R_{merge} (%)	7.6 (30.2)	6.5 (35.7)	6.7 (43.8)
I/σI	14.5 (2.7)	17.1 (2.6)	19.7 (2.9)
Number of reflections	37,023	43,982	64,292
Completeness (%)	93 (76)	92 (72)	96 (88)
R factor (%)	18.3 (26.8)	18.3 (29.6)	17.2 (23.6)
Free *R* factor (%)	21.5 (31.1)	21.3 (29.3)	20.0 (26.3)
rms deviation in bond lengths (Å)	0.005	0.005	0.011
rms deviation in bond angles (°)	1.2	1.2	1.6
PDB accession code	4J7L	4J7M	4J7N

[a]The numbers in parentheses are for the highest resolution shell.

The second guanosine group of the cap is packed against the wall of the active site pocket, leaving no room to attach another nucleotide to the 3′ hydroxyl group of its ribose (Figure 4C). Therefore, this guanosine group is not in a productive binding mode in this complex and needs to assume a different conformation in the complex with the (m^7)GpppG-RNA substrate.

Mutagenesis Studies Support the Structural Observations

To assess the importance of residues in the active site region of DXO, we created the following structure-based mutants (Figure S1): K273A, R294A, and K273A-R294A (interacting with the backbone phosphate; Figure 3C), Q280A (interacting with the 5′ end phosphate of the substrate; Figure 3G), Y189A (interacting with the ribose of U_2; Figure 3C), H272A, and R145A (interacting with U_6 at the opening of the active site pocket; Figure 3C). The Q173A mutant was created as a control, which is located far from the active site.

The K273A, R294A, and Y189A substitutions led to reduced exonuclease activity, whereas the K273A-R294A, E234A, and Q280A mutants ablated exonuclease activity (Figure 4E). The H272A and R145A mutants at the opening of the active site retain a majority of the WT exonuclease activity. The effects of these mutations on decapping activity mostly follow those for exonuclease activity; one exception being that the Y189A mutant had essentially normal decapping activity (Figure 4F). Overall, our structural observations provide the molecular framework for the decapping, PPH, and exonuclease activities of DXO.

DXO Preferentially Functions on Defectively Capped Pre-mRNAs In Vivo

Having established the biochemical activities and the molecular mechanism of DXO, we next characterized the functions of this protein in mammalian 293T cells with an shRNA-directed >95% reduction of DXO (DXO^{KD}; Figure S6). Our previous studies with Rai1 and Dxo1 showed that the two proteins mediate the clearance of incompletely capped mRNA in yeast cells (Jiao et al., 2010, Chang et al., 2012). Using primer pairs that span two different exons to detect spliced mRNA from two randomly selected mRNAs, CamKI and Fhit, we observed only a modest 20% increase in the steady-state levels of these mRNAs between control and DXO^{KD} cells (Figure 5A). However, analysis of the pre-mRNAs of the same genes revealed a more dramatic accumulation in the DXO^{KD} cells. Using primers that span the exon 1-intron 1 junction to detect unspliced, intron 1-containing RNAs, we observed a 2-fold increase of both CamKI and Fhit pre-mRNAs under reduced DXO levels (Figure 5B). Because a link between capping and splicing of the first intron (but not subsequent introns) has been reported (Edery and Sonenberg, 1985; Izaurralde et al., 1994; Konarska et al., 1984), we next tested whether the increased level of pre-mRNA in the DXO^{KD} cells was restricted to splicing of just the first intron. Surprisingly, the increase in CamKI and Fhit pre-mRNA levels were also detected when several different downstream unspliced introns were assessed (Figure 5B), demonstrating that unspliced pre-mRNAs accumulate in DXO^{KD} cells. These findings demonstrate an unexpected link of the capping process to splicing beyond only the first intron. Moreover, analysis of whether these transcripts are properly polyadenylated by quantitative RT-PCR (qRT-PCR) amplification through the poly(A) addition site shows an increase in uncleaved 3′ ends for both genes in the DXO^{KD} cells relative to control cells (Figure 5C), suggesting a defect in the cleavage reaction of 3′ end processing in DXO^{KD} cells. Collectively, these data indicate a role for DXO in degrading unprocessed pre-mRNAs and demonstrate an important link of an endogenously produced, defectively capped pre-mRNA with defective processing.

The preferential function of DXO on incompletely capped RNAs (Figures 1 and 2) and earlier in vitro demonstrations that suggested the polyadenylation cleavage step was facilitated by the mRNA cap (Cooke and Alwine, 1996; Flaherty et al., 1997; Gilmartin et al., 1988; Hart et al., 1985) indicate that the increase in pre-mRNA observed in Figures 5B and 5C would correspond to incompletely capped pre-mRNAs. To test this hypothesis, we resolved methyl-capped or incompletely capped RNA populations with anticap immunoprecipitation under conditions that retain methyl-capped, but not unmethyl-capped

(G) Interactions between the first two nucleotides of pU(S)6 with DXO. The oligo is shown in light blue, and the Ca^{2+} ion is shown as a sphere in brown. The red X indicates the expected position of a water or hydroxide ion to initiate hydrolysis based on the observed conformation of the phosphorothioate group.
(H) Overlay of the structures of the pU(S)6 and pU5 complexes in the active site region of DXO. The pU(S)6 oligo is shown in light blue, and pU5 is shown in black. DXO in the pU(S)6 complex is shown in color, and DXO in the pU5 complex is shown in gray. The red arrow indicates the O_5-P bond, and the two phosphate groups differ by a ~60° rotation around this bond. The m^7Gpp portion of the methylated cap (see Figure 4 for more information) is also shown (gray). All the structure figures were produced with PyMOL (www.pymol.org).

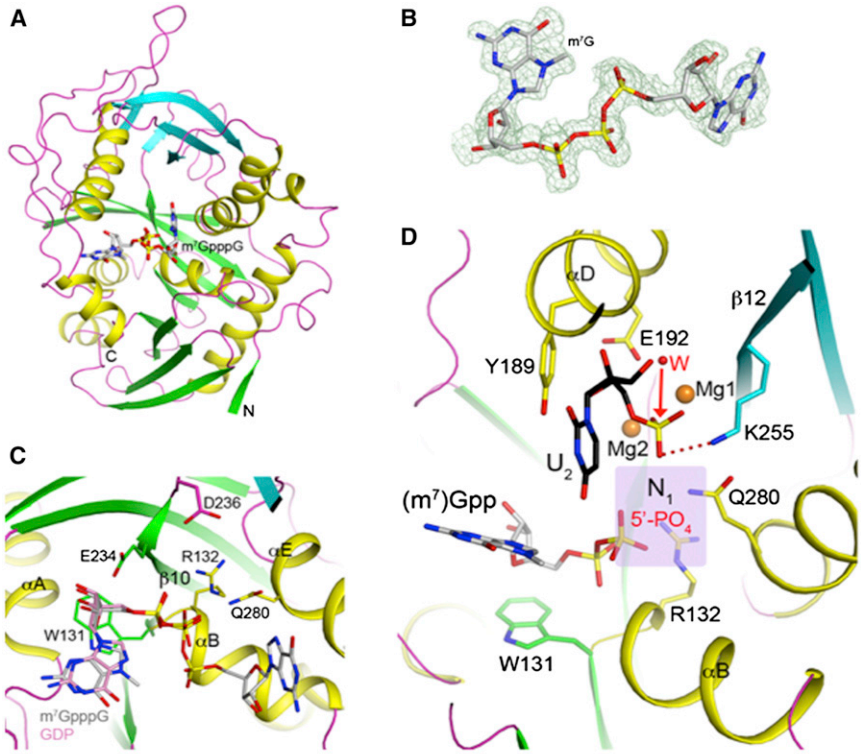

Figure 4. Crystal Structure of Wild-Type Murine DXO in Complex with the m^{7}GpppG Cap

(A) A schematic drawing of the structure of DXO (in green for the large β sheet, cyan for the small β sheet, yellow for the helices, and magenta for the loops) in complex with the m^{7}GpppG cap (in gray for carbon atoms).

(B) Simulated annealing omit F_o–F_c electron density at a resolution of 1.5 Å for m^{7}GpppG contoured at 3σ.

(C) Interactions between the m^{7}GpppG cap with the DXO active site.

(D) Overlay of the structures of DXO in complex with pU5 (in black) and two Mg^{2+} ions (orange) and m^{7}Gpp (gray).

(E) The indicated DXO WT and mutant proteins were incubated with 5′ end monophosphate 30 nt RNA substrate labeled at the 3′ end with the fluorophore FAM. The remaining RNA fragments were resolved by 15% denaturing PAGE and visualized under UV light, confirming the distributive 5′-to-3′ exonuclease activity.

(F) The indicated DXO WT and mutant proteins were tested for decapping activity. Methyl-capped RNA labeled with ^{32}P at the 5′ end was used in decapping reactions. Reaction conditions and labeling are as described in Figure 1.

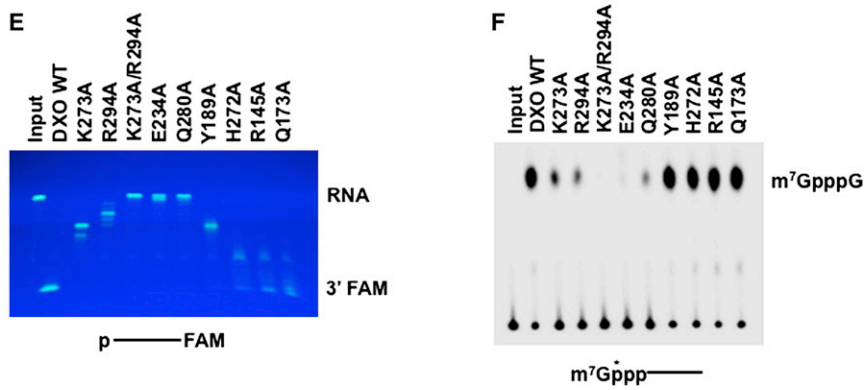

or uncapped, RNAs (Figure 5D) (Chang et al., 2012; Jiao et al., 2010). As expected, the level of methyl-capped mature CamKI and Fhit mRNAs were comparable between control and DXO^{KD} cells (Figure 5E). In contrast, a significant decrease in the level of methyl-capped pre-mRNAs was detected in the DXO^{KD} cells relative to the corresponding total pre-mRNA when compared to that observed in control cells (Figure 5F). The relative decrease in methyl-capped pre-mRNA as a proportion of the total pre-mRNA in the DXO^{KD} cells indicates a corresponding increase of defectively capped pre-mRNAs relative to total pre-mRNA.

To determine whether the increased level of pre-mRNAs in the DXO^{KD} cells could be attributed to pre-mRNA stability, we characterized the effect of DXO on a short-lived mRNA, c-*fos*. Similar to CamKI and Fhit, levels of c-*fos* pre-mRNA also increased in the DXO^{KD} cells (Figure 6A), whereas methyl-capped pre-mRNA decreased (Figure 6B), corresponding to an increase in defectively capped pre-mRNAs. Moreover, as would be predicted from the above data, DXO selectively influenced the stability of the c-*fos* pre-mRNA, but not of the c-*fos* mRNA, after actinomycin D-directed transcriptional silencing (Figure 6C). The stability of the c-*fos* pre-mRNA increased >5-fold in DXO^{KD} cells relative to control cells, with a $t_{1/2}$ of 130 min versus 25 min in controls. A similar increase was not detected with the c-*fos* mRNA, indicating that DXO preferentially functions on pre-mRNAs lacking a normal m^{7}G cap at the 5′ end.

DISCUSSION

Here, we report that the mammalian Dom3Z/DXO protein is a dual nuclease that preferentially functions on incompletely capped pre-mRNAs. DXO removes the entire cap structure to generate a 5′ end monophosphate that subsequently serves as a substrate for a second catalytic activity intrinsic to the same DXO active site, a 5′-to-3′ exoribonuclease activity, to degrade the RNA body, and defectively capped RNAs accumulate in DXO^{KD} cells. These findings reinforce our recent demonstrations in *S. cerevisiae* (Chang et al., 2012; Jiao et al., 2010) that show

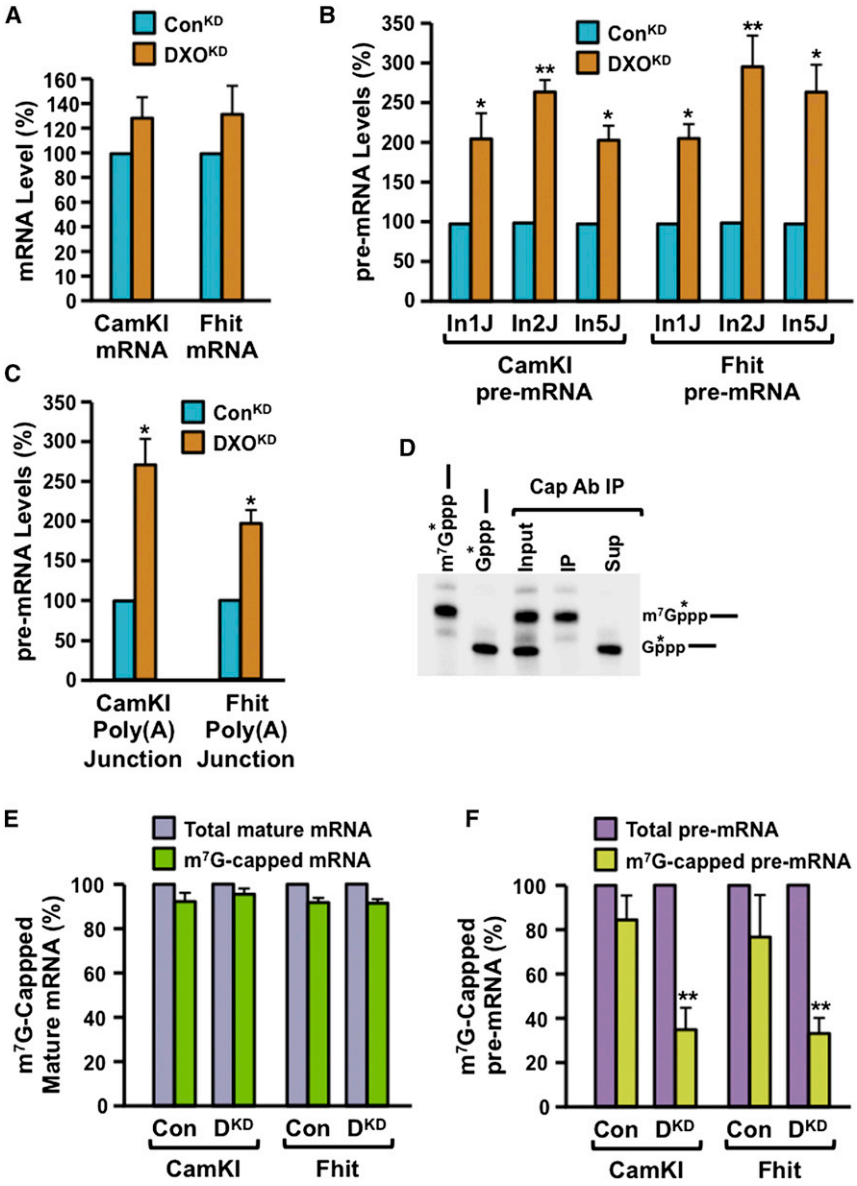

Figure 5. DXO Preferentially Functions to Clear Incompletely Capped Pre-mRNAs in Cells

(A) Total RNA isolated from control shRNA expressing (Con^{KD}) or DXO-specific shRNA expressing (DXO^{KD}) cells were subjected to qRT-PCR analysis with primers specific to the CamKI and Fhit mRNA. Values were normalized to the GAPDH mRNA and plotted relative to control shRNA, which was arbitrarily set to 100.

(B) The relative levels of CamKI and Fhit pre-mRNA in Con^{KD} and DXO^{KD} cells were quantified with primers that span intron-exon junctions 1, 2, and 5 (In1J, In2J, and In5J, respectively). The level in Con^{KD} cells was arbitrarily set to 100.

(C) Total RNA isolated from Con^{KD} and DXO^{KD} cells subjected to qRT-PCR analysis with primers that span the CamKI and Fhit gene poly(A) addition site were used to determine the relative level of unpolyadenylated transcripts in DXO^{KD} cells. Levels in the Con^{KD} cells were arbitrarily set to 100.

(D) Methyl-capped RNAs were purified with monoclonal antitrimethylguanosine antibody column under conditions that resolve methyl-capped RNAs from incompletely capped RNAs, as described previously (Chang et al., 2012; Jiao et al., 2010). We spiked 0.5 μg of total 293T RNA with in vitro-generated N7-methylated and unmethylated cap-labeled RNAs prior to capped RNA affinity purification. RNAs bound or unbound to the column were isolated and resolved by denaturing urea PAGE. The identity of the individual RNAs used, the input mixture, and the resulting resolved RNAs are indicated.

(E and F) Methyl-capped RNAs were purified with monoclonal the antitrimethylguanosine antibody column as in (D) (Chang et al., 2012; Jiao et al., 2010), and the levels of methyl-capped CamKI and Fhit mRNA (E) or pre-mRNA (F) were quantified by qRT-PCR and presented relative to the corresponding total level of mRNA or pre-mRNA, respectively. Levels of the corresponding total mRNA were arbitrarily set to 100.

Data in all four panels were derived from at least three independent experiments, and the error bars represent ± SD. *, $p < 0.05$; **, $p < 0.01$.

that cap addition is not a default process that always proceeds to completion. Importantly, our data also reveal that pre-mRNAs in mammalian cells with an aberrant 5′ end do not efficiently proceed into the normal RNA-processing pathways of splicing and polyadenylation. The lack of efficient processing of incompletely capped pre-mRNAs that are more apparent after DXO knockdown implicates DXO in a pre-mRNA quality control mechanism that detects and degrades defective pre-mRNAs (summarized in Figure 7).

Biochemical Activities of DXO

Thus far, we have identified two fungal proteins that possess decapping activity on incompletely capped mRNAs: the nuclear Rai1 protein (Jiao et al., 2010; Xiang et al., 2009) and the previously uncharacterized Ydr370C gene product, which encodes the predominantly cytoplasmic Dxo1 protein (Chang et al., 2012). On the basis of sequence homology, DXO was initially proposed to be the mammalian homolog of Rai1 (Xue et al., 2000); however, structural analysis reveals that all three proteins share extensive structural identity (Chang et al., 2012; Xiang et al., 2009), and biochemical studies suggest that DXO is a hybrid of both fungal proteins. In vitro, Rai1 functions on unmethyl-capped RNA (*GpppRNA*) and 5′ pppRNA (Jiao et al., 2010; Xiang et al., 2009). Dxo1 functions on methylated (*m^7GpppRNA*) and unmethylated (*GpppRNA*) capped RNA but not on 5′ pppRNA, whereas DXO can function on all three substrates (Figure 1). Both Dxo1 and DXO possess intrinsic 5′-to-3′ exonuclease activity (Chang et al., 2012; Figure 1). One unanimous function for all three proteins is their preferential decapping of GpppRNA (summarized in Table S1). Collectively,

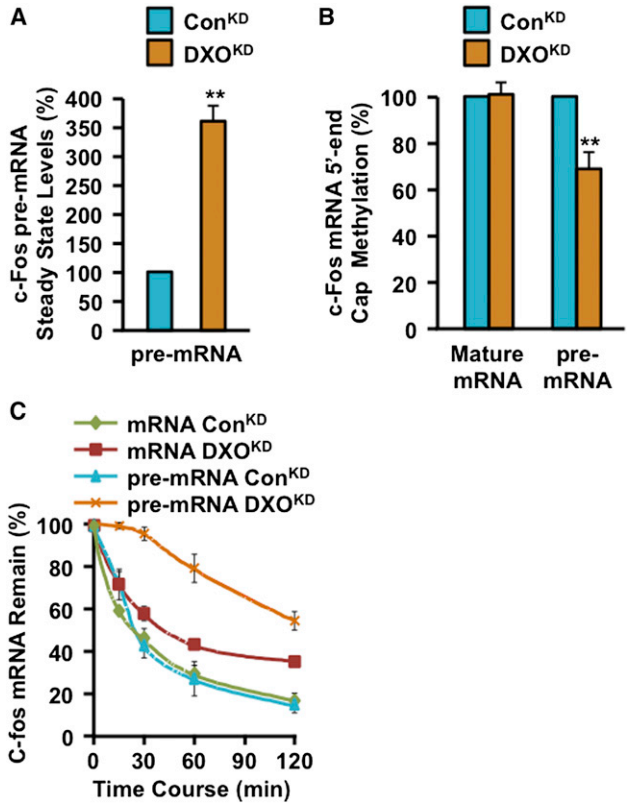

Figure 6. Defectively Capped c-*fos* Pre-mRNAs Were Stabilized in the Absence of DXO in Cells

(A) Steady-state levels of c-*fos* pre-mRNA in 293T cells expressing control shRNA (Con^{KD}) or DXO-specific shRNA (DXO^{KD}) were determined by qRT-PCR with primers that span the intron 1-exon 2 junction and are presented relative to GAPDH mRNA levels. Levels of c-*fos* pre-mRNA in the Con^{KD} cells were arbitrarily set to 1.

(B) Methyl-capped RNAs were isolated as in Figures 5D–5F from Con^{KD} and DXO^{KD} cells and levels of mature c-*fos* mRNA determined with primers that span exons 1 and 2 and c-*fos* pre-mRNA as in (A). A reduced level of methyl-capped c-*fos* pre-mRNA was detected in the DXO^{KD} cells.

(C) The stability of c-*fos* mRNA and pre-mRNA was determined in the indicated cells following actinomycin D transcriptional arrest. Data are presented relative to corresponding levels of GAPDH mRNA.

Data in all three panels were derived from three independent assays ± SD, as denoted by the error bars.

Rai1, Dxo1, and DXO identify a class of proteins that function in a quality control mechanism to ensure proper mRNA 5′ end fidelity wherein DXO preferentially functions to contain incompletely capped pre-mRNAs (Figure 7).

Molecular Basis of the Distinct DXO Catalytic Activities

The structures of the pU5, pU(S)6, and cap complexes provide elegant insights into the catalytic mechanism of DXO and related enzymes and indicate that the three distinct catalytic activities are mediated by the same active site machinery. The pU5 RNA is bound as a product, mimicking the RNA body. The 5′ end phosphate group of pU5 is the scissile phosphate, which is recognized by the enzyme through two metal ions. The catalytic nucleophile is a water molecule or hydroxide ion, bound and activated by one of the metal ions, most likely the sole water ligand of Mg1 in the pU5 complex, which is also activated by Glu192 (Figure 3E). This water molecule is located about 3.9 Å from the phosphorus atom and is at the correct position for an inline attack. The terminal oxygen atom opposite of this water molecule is then the leaving group, and the oxyanion can be stabilized by the side chain of Lys255 (motif IV) (Figure 4D). This two-metal-ion mechanism is similar to that employed by many other nucleases (Yang, 2011).

The structure shows that the cap (m^7GpppG) is accommodated on the other side of the catalytic machinery from the RNA body (the pU5 oligo) (Figure 4D), thereby explaining the decapping activity that removes (m^7)GpppG. Similarly, the structure of the pU(S)6 complex shows that the 5′ end nucleotide (pN_1) or pyrophosphate group can also be accommodated across the active site (Figure 4D), giving rise to 5′-to-3′ exonuclease or PPH activity. Therefore, the three catalytic activities of these enzymes use the same catalytic machinery, and it is the distinct binding modes of the three different substrates that dictate the outcome of the reaction. Nevertheless, each of the DXO, Rai1, and Dxo1 enzymes also has its unique properties, such as the lack of PPH activity by Dxo1 and the selectivity between GpppRNA and m^7GpppRNA by Rai1 and Dxo1 (Chang et al., 2012; Xiang et al., 2009). Additional studies will be needed in order to define the molecular mechanism for these unique properties.

DXO in Methyl-Capped mRNA Decapping

The ability of DXO to function on m^7G capped RNA in vitro (Figure 1) indicates that DXO may also contribute to m^7G-capped RNA decapping and decay. The finding that cap-binding proteins can efficiently inhibit DXO activity (Figure 2) suggests that any such activity is most likely regulated and would require the removal of cap-binding proteins. The modest 20% increase in mRNA levels observed in the DXO^{KD} cells (Figure 3A) is consistent with a potential limited role on m^7G-capped mRNAs. In addition, the nuclear localization of DXO (Zheng et al., 2011) and its function on $m^{2,2,7}$G-capped RNA (Figure 1) also indicates that DXO may modulate trimethyl-capped uridylate-rich small nuclear RNAs (UsnRNAs). Future studies will address this possibility.

m^7G Cap and Pre-mRNA Processing

Our finding that incompletely capped pre-mRNAs are inefficiently spliced and polyadenylated demonstrates that the cap is more intimately linked to splicing and polyadenylation than previously perceived. Initial studies that established a link between the cap and first intron splicing (Edery and Sonenberg, 1985; Inoue et al., 1989; Izaurralde et al., 1995; Izaurralde et al., 1994; Konarska et al., 1984) either utilized m^7G-capped mRNA with a depleted cap-binding protein or introduced unmethyl-capped pre-mRNA. In all cases, a requirement for the cap-binding protein was observed for first intron splicing, which was consistent with the exon definition of splicing (Colot et al., 1996; Fortes et al., 1999; Izaurralde et al., 1994; Lewis et al., 1996). An important distinction with the current study is that we are following nascent transcripts that are generated without a proper cap. An appealing model could be that cotranscriptional cap addition is required to facilitate subsequent pre-mRNA

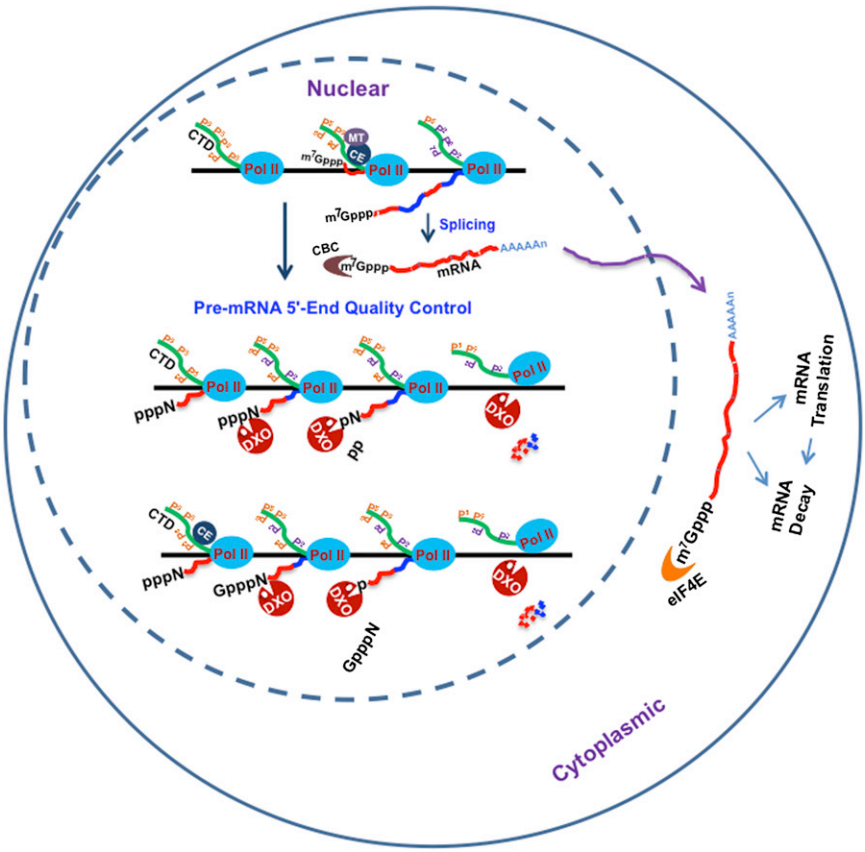

Figure 7. Model of 5′ End Quality Control in Mammalian Cells

Incompletely 5′ end-capped pre-mRNA (unmethyl-capped and uncapped 5′ triphosphate pre-mRNA) would be preferentially detected by DXO and subjected to 5′ end cleavage and degradation. The RNA polymerase II (Pol II), the carboxyl terminal domain of RNAP II (CTD), the triphosphatase-guanylyltransferase capping enzyme (CE), the methyltransferase (MT), the nuclear CBC, and the cytoplasmic cap binding protein eIF4E are as indicated.

processing and implies a cotranscriptional coordination of the capping process with splicing and polyadenylation factors to dictate pre-mRNA processing. One candidate that can coordinate these processes could be the cap-binding complex (CBC), which cotranscriptionally associates with the capped 5′ end and indirectly affects the alternative splicing of a subset of genes in a transcript-specific manner (Lenasi et al., 2011). Whether the CBC is necessary and involved in recruiting splicing factors to intron-containing genes remains to be determined.

Our data reveal that incompletely capped pre-mRNAs do not efficiently proceed into the normal RNA processing pathways of splicing and polyadenylation and, instead, appear to be degraded by DXO. Importantly, such a quality control mechanism provides a dual layer of surveillance to prevent the accumulation of potentially deleterious defectively capped pre-mRNAs, whereby they are inefficiently processed into mature mRNA and selectively decapped and degraded by DXO from the 5′ end. Future studies will begin to uncover the molecular mechanism underlying such a surveillance process.

EXPERIMENTAL PROCEDURES

Plasmids and Recombinant Protein Expression

Mutagenesis

Structure-based, site-specific mutations were created by PCR-based methods with the use of the QuikChange Site-Directed Mutagenesis Kit (Stratagene) and sequenced for confirmation of correct incorporation of the mutations.

Protein Expression, Purification, and Crystallization

The protocols for the expression, purification, and crystallization of mouse DXO have been previously reported (Xiang et al., 2009). The mutant proteins were purified by Ni-NTA Superflow (QIAGEN) and gel filtration chromatography, through the same protocol as that used for the WT enzyme. Free enzyme crystals of DXO were obtained with the sitting-drop vapor diffusion method at 20°C with a reservoir solution containing 20% (w/v) PEG 3350. The pU5-Mg^{2+} complex was obtained by soaking the free enzyme crystals with 10 mM pU5 and 10 mM $MgCl_2$ for 90 min in the presence of 15% ethylene glycol. The pU(S)6-Ca^{2+} complex was obtained by soaking DXO crystals with 10 mM pU(S)6 and 20 mM $CaCl_2$ for 120 min in the presence of 15% ethylene glycol. The m^7GpppG complex was obtained by soaking DXO crystals with 5 mM m^7GpppG for 30 min in the presence of 15% ethylene glycol. Crystals were flash frozen in liquid nitrogen for diffraction analysis and data collection at 100 K.

Data Collection and Structure Determination

X-ray diffraction data were collected at the National Synchrotron Light Source (NSLS) beamline X29A. The diffraction images were processed and scaled with the HKL package (Otwinowski and Minor, 1997). The crystals belong to space group $P2_1$, with cell parameters of a = 50.0 Å, b = 87.7 Å, c = 53.9 Å, and β = 112.2°. There is one molecule of DXO in the crystallographic asymmetric unit. The structure refinement was carried out with the Crystallography and NMR System (CNS) (Brünger et al., 1998). The atomic model was built with the Coot (Crystallographic Object-Oriented Toolkit) program (Emsley and Cowtan, 2004). The crystallographic information is summarized in Table 1.

Cell Culture and Generation of Stably Transformed Knockdown Cell Line

Human embryonic kidney 293T cells were obtained from ATCC and cultured according to the supplier's protocol. DXO-specific small hairpin RNA (shRNA) plasmid and control nonspecific shRNA plasmids were obtained from Sigma-Aldrich, and transfections were carried out with Lipofectamine 2000 (Invitrogen) according to the manufacturer's protocol. Monoclonal lines of stably transformed DXO cells expressing DXO-specific shRNA (DXO^{KD}) were selected with puromycin (3 μg/ml) and confirmed by western blotting.

RNA Generation

RNA corresponding to the pcDNA3 polylinker (pcP) region with a 3′end containing 16 guanosines was transcribed in vitro with T7 polymerase for the generation of pcP RNA with an N7-methylated or -unmethylated 5′ cap or no cap at all, as previously described (Chang et al., 2012; Jiao et al., 2010). Trimethylated ^{32}P-cap-labeled pcP RNA was generated in the capping reaction in the presence of human recombinant trimethyltransferase (Benarroch

et al., 2010) and *S*-adenosyl methionine. We generated 3′ end ^{32}P-labeled RNA with T4 RNA Ligase and [^{32}P]pCp (Wang and Kiledjian, 2000a). In vitro transcriptions were carried out in the presence of [γ^{32}P]GTP for 5′ end ^{32}P-labeled triphosphate RNA or with [α^{32}P]GTP to obtain ^{32}P-uniform-labeled RNAs as described previously (Jiao et al., 2006). We generated 5′-monophosphate ^{32}P-uniform-labeled RNAs by digesting methyl-capped ^{32}P-uniform-labeled RNA with a human Dcp2 decapping enzyme. RNA lacking a phosphate at the 5′ end was generated by treating ^{32}P-uniform-labeled triphosphate RNA with calf intestinal alkaline phosphatase. Fluorescently labeled RNA oligos (Chang et al., 2012) were purchased from Integrated DNA Technologies (IDT).

RNA Decapping and In Vitro Decay Assay

Decapping reactions used either His-tagged mouse DXO WT or mutant recombinant protein (25 nM), and were carried out by incubating with ^{32}P-cap-labeled or ^{32}P-5′end-labeled pcP RNAs in decapping buffer, as previously described (Jiao et al., 2010), at 37°C for 30 min. Exoribonuclease assays were carried out with 100 nM His-DXO in the same buffer. The decapping products were resolved by polyethyleneimine-cellulose thin-layer chromatography (PEI-TLC) plates, and the decay reactions were resolve by 5% denaturing polyacrylamide gel electrophoresis.

Exonuclease Assays with Fluorescently Labeled RNA

The 3′-FAM-labeled 30-mer RNA with 5′ end monophosphate (Sinturel et al., 2009) and the equivalent ssDNA oligos were purchased from IDT. Exonuclease assays were performed at 37°C for 30 min with reaction mixtures containing 30 mM Tris (pH 8.0), 50 mM NH_4Cl, 2 mM $MgCl_2$, 0.5 mM dithiothreitol, 25 μg ml^{-1} BSA, 2 μM 3′-FAM-labeled oligos, and the indicated amount of recombinant DXO. The products were fractionated by 5% denaturing polyacrylamide gel and visualized on a UV illuminator. Assays were repeated at least three times to ensure reproducibility.

RNA Isolation

Total RNAs were isolated with Trizol reagent (Invitrogen) under the manufacturer's protocol and treated with RQ1 DNase (Promega) for removal of the genomic DNA contamination. For mRNA in vivo stability assay, the transcriptions of 293T control or DXO^{KD} cells were blocked by actinomycin D (5 μg/ml). Cells were harvested at the indicated time points after treatment.

Methyl-Capped RNA Immunoprecipitation

Methyl-capped RNAs were immunoprecipitated with monoclonal antitrimethylguanosine antibody column (Calbiochem), as previously described (Chang et al., 2012; Jiao et al., 2010), from 30 ng ribosomal RNA (rRNA) minus RNA with one round of immunoprecipitation. rRNA depletion was carried out from 0.5 μg total RNA with the RiboMinus Eukaryote Kit (Invitrogen).

Real-Time qRT- PCR

RNAs were reverse transcribed into complementary DNA with random primers and M-MLV Reverse Transcriptase (Promega) according to the manufacturer's protocol. For detection of pre-mRNA, the reverse transcription was preformed with gene-specific pre-mRNA primers. Real-time PCR was performed with iTaq Supermix (Bio-Rad) on the ABI Prism 7900HT sequence detection system (Invitrogen) (Jiao et al., 2006; Jiao et al., 2010). Each gene was amplified with the appropriate specific primers (Table S2). mRNA levels were computed by the comparative Ct method and normalized to internal control 18S rRNA or glyceraldehyde 3-phosphate dehydrogenase mRNA.

ACCESSION NUMBERS

The atomic coordinates have been deposited at the Protein Data Bank at accession numbers 4J7L, 4J7M, and 4J7N.

SUPPLEMENTAL INFORMATION

Supplemental Information contains Supplemental Experimental Procedures, six figures, and two tables and can be found with this article online at http://dx.doi.org/10.1016/j.molcel.2013.02.017.

ACKNOWLEDGMENTS

We thank S. Shuman (The Memorial Sloan-Kettering Cancer Center) for providing the expression plasmid for the trimethyltransferase. This research was supported by grants GM090059 (to L.T.) and GM067005 (to M.K.) from the National Institutes of Health.

Received: September 28, 2012
Revised: January 24, 2013
Accepted: February 14, 2013
Published: March 21, 2013

REFERENCES

Benarroch, D., Jankowska-Anyszka, M., Stepinski, J., Darzynkiewicz, E., and Shuman, S. (2010). Cap analog substrates reveal three clades of cap guanine-N2 methyltransferases with distinct methyl acceptor specificities. RNA *16*, 211–220.

Brünger, A.T., Adams, P.D., Clore, G.M., DeLano, W.L., Gros, P., Grosse-Kunstleve, R.W., Jiang, J.S., Kuszewski, J., Nilges, M., Pannu, N.S., et al. (1998). Crystallography & NMR system: A new software suite for macromolecular structure determination. Acta Crystallogr. D Biol. Crystallogr. *54*, 905–921.

Calero, G., Wilson, K.F., Ly, T., Rios-Steiner, J.L., Clardy, J.C., and Cerione, R.A. (2002). Structural basis of m7GpppG binding to the nuclear cap-binding protein complex. Nat. Struct. Biol. *9*, 912–917.

Chang, J.H., Jiao, X., Chiba, K., Oh, C., Martin, C.E., Kiledjian, M., and Tong, L. (2012). Dxo1 is a new type of eukaryotic enzyme with both decapping and 5′-3′ exoribonuclease activity. Nat. Struct. Mol. Biol. *19*, 1011–1017.

Colot, H.V., Stutz, F., and Rosbash, M. (1996). The yeast splicing factor Mud13p is a commitment complex component and corresponds to CBP20, the small subunit of the nuclear cap-binding complex. Genes Dev. *10*, 1699–1708.

Cooke, C., and Alwine, J.C. (1996). The cap and the 3′ splice site similarly affect polyadenylation efficiency. Mol. Cell. Biol. *16*, 2579–2584.

Decker, C.J., and Parker, R. (1993). A turnover pathway for both stable and unstable mRNAs in yeast: evidence for a requirement for deadenylation. Genes Dev. *7*, 1632–1643.

Dunckley, T., and Parker, R. (1999). The DCP2 protein is required for mRNA decapping in Saccharomyces cerevisiae and contains a functional MutT motif. EMBO J. *18*, 5411–5422.

Edery, I., and Sonenberg, N. (1985). Cap-dependent RNA splicing in a HeLa nuclear extract. Proc. Natl. Acad. Sci. USA *82*, 7590–7594.

Emsley, P., and Cowtan, K. (2004). Coot: model-building tools for molecular graphics. Acta Crystallogr. D Biol. Crystallogr. *60*, 2126–2132.

Fischer, P.M. (2009). Cap in hand: targeting eIF4E. Cell Cycle *8*, 2535–2541.

Flaherty, S.M., Fortes, P., Izaurralde, E., Mattaj, I.W., and Gilmartin, G.M. (1997). Participation of the nuclear cap binding complex in pre-mRNA 3′ processing. Proc. Natl. Acad. Sci. USA *94*, 11893–11898.

Fortes, P., Kufel, J., Fornerod, M., Polycarpou-Schwarz, M., Lafontaine, D., Tollervey, D., and Mattaj, I.W. (1999). Genetic and physical interactions involving the yeast nuclear cap-binding complex. Mol. Cell. Biol. *19*, 6543–6553.

Furuichi, Y., and Shatkin, A.J. (2000). Viral and cellular mRNA capping: past and prospects. Adv. Virus Res. *55*, 135–184.

Ghosh, A., and Lima, C.D. (2010). Enzymology of RNA cap synthesis. Wiley Interdiscip Rev RNA *1*, 152–172.

Gilmartin, G.M., McDevitt, M.A., and Nevins, J.R. (1988). Multiple factors are required for specific RNA cleavage at a poly(A) addition site. Genes Dev. *2*, 578–587.

Gingras, A.C., Raught, B., and Sonenberg, N. (1999). eIF4 initiation factors: effectors of mRNA recruitment to ribosomes and regulators of translation. Annu. Rev. Biochem. *68*, 913–963.

Goodfellow, I.G., and Roberts, L.O. (2008). Eukaryotic initiation factor 4E. Int. J. Biochem. Cell Biol. *40*, 2675–2680.

Hart, R.P., McDevitt, M.A., and Nevins, J.R. (1985). Poly(A) site cleavage in a HeLa nuclear extract is dependent on downstream sequences. Cell *43*, 677–683.

Hsu, C.L., and Stevens, A. (1993). Yeast cells lacking 5′—>3′ exoribonuclease 1 contain mRNA species that are poly(A) deficient and partially lack the 5′ cap structure. Mol. Cell. Biol. *13*, 4826–4835.

Inoue, K., Ohno, M., Sakamoto, H., and Shimura, Y. (1989). Effect of the cap structure on pre-mRNA splicing in Xenopus oocyte nuclei. Genes Dev. *3*, 1472–1479.

Izaurralde, E., Lewis, J., McGuigan, C., Jankowska, M., Darzynkiewicz, E., and Mattaj, I.W. (1994). A nuclear cap binding protein complex involved in pre-mRNA splicing. Cell *78*, 657–668.

Izaurralde, E., Lewis, J., Gamberi, C., Jarmolowski, A., McGuigan, C., and Mattaj, I.W. (1995). A cap-binding protein complex mediating U snRNA export. Nature *376*, 709–712.

Jiao, X., Wang, Z., and Kiledjian, M. (2006). Identification of an mRNA-decapping regulator implicated in X-linked mental retardation. Mol. Cell *24*, 713–722.

Jiao, X., Xiang, S., Oh, C., Martin, C.E., Tong, L., and Kiledjian, M. (2010). Identification of a quality-control mechanism for mRNA 5′-end capping. Nature *467*, 608–611.

Konarska, M.M., Padgett, R.A., and Sharp, P.A. (1984). Recognition of cap structure in splicing in vitro of mRNA precursors. Cell *38*, 731–736.

Lenasi, T., Peterlin, B.M., and Barboric, M. (2011). Cap-binding protein complex links pre-mRNA capping to transcription elongation and alternative splicing through positive transcription elongation factor b (P-TEFb). J. Biol. Chem. *286*, 22758–22768.

Lewis, J.D., Izaurralde, E., Jarmolowski, A., McGuigan, C., and Mattaj, I.W. (1996). A nuclear cap-binding complex facilitates association of U1 snRNP with the cap-proximal 5′ splice site. Genes Dev. *10*, 1683–1698.

Li, Y., Song, M., and Kiledjian, M. (2011). Differential utilization of decapping enzymes in mammalian mRNA decay pathways. RNA *17*, 419–428.

Liu, H., and Kiledjian, M. (2006). Decapping the message: a beginning or an end. Biochem. Soc. Trans. *34*, 35–38.

Lykke-Andersen, J. (2002). Identification of a human decapping complex associated with hUpf proteins in nonsense-mediated decay. Mol. Cell. Biol. *22*, 8114–8121.

Marcotrigiano, J., Gingras, A.C., Sonenberg, N., and Burley, S.K. (1997). Cocrystal structure of the messenger RNA 5′ cap-binding protein (eIF4E) bound to 7-methyl-GDP. Cell *89*, 951–961.

Matsuo, H., Li, H., McGuire, A.M., Fletcher, C.M., Gingras, A.C., Sonenberg, N., and Wagner, G. (1997). Structure of translation factor eIF4E bound to m7GDP and interaction with 4E-binding protein. Nat. Struct. Biol. *4*, 717–724.

Mazza, C., Segref, A., Mattaj, I.W., and Cusack, S. (2002). Large-scale induced fit recognition of an m(7)GpppG cap analogue by the human nuclear cap-binding complex. EMBO J. *21*, 5548–5557.

Merrick, W.C. (2004). Cap-dependent and cap-independent translation in eukaryotic systems. Gene *332*, 1–11.

Meyer, S., Temme, C., and Wahle, E. (2004). Messenger RNA turnover in eukaryotes: pathways and enzymes. Crit. Rev. Biochem. Mol. Biol. *39*, 197–216.

Otwinowski, Z., and Minor, W. (1997). Processing of X-ray diffraction data collected in oscillation mode. Methods Enzymol. *276*, 307–326.

Shatkin, A.J. (1976). Capping of eucaryotic mRNAs. Cell *9*, 645–653.

Sinturel, F., Pellegrini, O., Xiang, S., Tong, L., Condon, C., and Bénard, L. (2009). Real-time fluorescence detection of exoribonucleases. RNA *15*, 2057–2062.

Song, M.G., Li, Y., and Kiledjian, M. (2010). Multiple mRNA decapping enzymes in mammalian cells. Mol. Cell *40*, 423–432.

Wang, Z., and Kiledjian, M. (2000a). Identification of an erythroid-enriched endoribonuclease activity involved in specific mRNA cleavage. EMBO J. *19*, 295–305.

Wang, Z., Jiao, X., Carr-Schmid, A., and Kiledjian, M. (2002). The hDcp2 protein is a mammalian mRNA decapping enzyme. Proc. Natl. Acad. Sci. USA *99*, 12663–12668.

Xiang, S., Cooper-Morgan, A., Jiao, X., Kiledjian, M., Manley, J.L., and Tong, L. (2009). Structure and function of the 5′—>3′ exoribonuclease Rat1 and its activating partner Rai1. Nature *458*, 784–788.

Xue, Y., Bai, X., Lee, I., Kallstrom, G., Ho, J., Brown, J., Stevens, A., and Johnson, A.W. (2000). Saccharomyces cerevisiae RAI1 (YGL246c) is homologous to human DOM3Z and encodes a protein that binds the nuclear exoribonuclease Rat1p. Mol. Cell. Biol. *20*, 4006–4015.

Yang, W. (2011). Nucleases: diversity of structure, function and mechanism. Q. Rev. Biophys. *44*, 1–93.

Zheng, D., Chen, C.Y., and Shyu, A.B. (2011). Unraveling regulation and new components of human P-bodies through a protein interaction framework and experimental validation. RNA *17*, 1619–1634.